

Chapter 3

Physical and Mechanical Properties of Ottawa F65 Sand



Mohamed El Ghoraiby, Hanna Park, and Majid T. Manzari

Abstract This paper presents the results of soil characterization and element tests of Ottawa F65 sand. The data presented is intended to be used as calibration material for the prediction exercise conducted as part of the Liquefaction Experiments and Analysis Project (LEAP 2017). The databank generated includes soil specific gravity tests, particle size analysis, hydraulic conductivity tests, maximum and minimum void ratio tests, and cyclic triaxial stress-controlled tests. An effort was made to ensure the consistency and repeatability of the test results by reducing the sources of variability in the sample preparations and increasing the number of tests. The uniformity of the soil was evaluated by conducting tests on samples from five different batches. The results showed that the sand is uniform among the five batches. Due to significant variability in previously reported maximum and minimum void ratio results, the effects of the test operator were studied by comparing test results obtained from three different operators. For the triaxial tests, a constant height dry pluviation method was used for sample preparation. To eliminate the effect of the human error in maintaining a constant drop height and to ensure consistency of the sand fabric between different samples, a device was developed to facilitate the sample preparation. The cyclic triaxial experiments were performed using three different soil densities, and a liquefaction strength curve was obtained for each density based on a 2.5% single amplitude axial strain criteria. The developed databank in this study was made publicly available for the community through DesignSafe.

3.1 Introduction

The Liquefaction Experiments and Analysis Project (LEAP) is a combined effort between several multinational research institutions to investigate the liquefaction phenomenon. As the project name suggests, the main objectives of LEAP is to

M. El Ghoraiby
The George Washington University, Washington, DC, USA

H. Park · M. T. Manzari (✉)
Department of Civil and Environmental Engineering, George Washington University,
Washington, DC, USA
e-mail: manzari@gwu.edu

generate a large database of centrifuge experiments which model the consequences of liquefaction on different geo-structures and to assess the capability of the current state of the art analytical tools to predict the response of liquefiable soil. A reliable assessment of the analytical tools is achieved through a blind prediction exercise (Type-B). In a Type-B prediction exercise, the modelers are given the centrifuge experiment geometry and the achieved density and base motion, and then they are required to model the soil response without prior knowledge of the experiment results. A databank for soil characterization and element tests is generated in order to aid the modelers in their model calibrations. Details of this databank are presented here.

Previous experimental studies were conducted for characterizing Ottawa F65 sand including cyclic triaxial as well as cyclic direct simple shear tests (Bastidas 2016; Vasko 2015; Vasko et al. 2018). Vasko (2015) conducted a series of triaxial experiments for the planning phase of LEAP (PLEAP). The data was used in a prediction exercise of centrifuge experiments performed during that phase (Manzari et al. 2017). In this database the cyclic triaxial tests were performed on a single soil density which is the test density. The sample preparation technique used was dry pluviation with minor tapping on the mold. Bastidas (2016) produced a database of monotonic and cyclic direct simple shear experiments. The performed experiments were conducted on two densities. Dry funnel deposition was the sample preparation method for the loose specimen, while air pluviation was used for dense soil.

The databank presented in this paper is intended for the LEAP 2017 phase of the project. The databank includes soil characterization tests such as specific gravity, particle size distribution, permeability, and maximum and minimum void ratio tests. Additionally, a cyclic triaxial stress-controlled testing program is conducted to obtain the liquefaction strength of the soil at various densities. The theme of the 2017 phase is to assess the sensitivity of the soil response to variations in soil density and input motion. As a result of this study, the centrifuge experiments would yield a range of response instead of a single point. In order to properly model these centrifuge experiments, the prediction exercise in LEAP 2017 dictates that the databank provided for model calibration to be of high quality.

The LEAP 2017 Laboratory experiment databank is intended to address the needs of the project. Maintaining a high level of consistency and repeatability was one of the main objectives. The consistency of the sample among different sand batches was addressed by obtaining samples from five different batches. In obtaining the soil permeability, a large number of experiments were conducted to produce a trend between the soil density and the permeability. Previously obtained maximum and minimum void ratios of the Ottawa F65 sand have shown large variation among the reporting research groups (Kutter et al. 2017). To address the source of variability, the maximum and minimum void ratio tests were conducted by three different operators to quantify the variation in the results and eliminate the operator effect.

For the triaxial testing program of LEAP 2017, a series of cyclic stress-controlled tests were conducted on Ottawa F65 sand samples at three different densities. The centrifuge experiments performed in the LEAP 2017 project were prepared using dry pluviation technique. To obtain a similar fabric as the centrifuge tests, a constant height dry pluviation sample preparation technique was used. The effect of human error in maintaining a constant drop height and achieving consistent fabric was

eliminated by using a device developed to facilitate the sample preparation. The liquefaction strength curves based on a 2.5% single amplitude axial strain criterion were produced from the performed tests.

The remainder of this paper is divided into two sections. The first addresses the soil characterization tests including the soil specific gravity, particle size distribution, hydraulic conductivity, and the maximum and minimum void ratio tests. For each test, the procedures are first presented followed by the results. The second section covers the cyclic triaxial testing program. The procedures for running the tests are first discussed followed by the sample preparation technique. The consistency of the samples produced is addressed by presenting the statistics of the sample measurement. Finally, the results obtained from the testing program are presented, followed by concluding remarks.

3.2 Ottawa F65 Soil Characterization

This section covers the characterization tests performed to obtain the Ottawa F65 properties. The tests include soil specific gravity tests, particle size analysis, soil permeability, and maximum and minimum void ratio tests. The tests were performed as per the ASTM standard testing procedures, and any additional steps taken or modifications are further discussed.

3.2.1 Specific Gravity Tests

The specific gravity tests were conducted in accordance with the ASTM D854 testing standard procedures. The sample de-aeration was achieved by subjecting the sample to a vacuum for at least 2 h. The results of the specific gravity were used as one way to confirm the sample uniformity and consistency among different sand batches. The tests were performed on samples obtained from five different sand batches. For each batch a series of six tests were conducted. Table 3.1 shows a summary of the results including the mean and coefficient of variation (COV).

An average specific gravity for Ottawa F65 sand of 2.65 was obtained with a mean coefficient of variation of 0.78%. Figure 3.1 shows a box plot of the spread of the specific gravity measurements from the average value for each soil batch.

3.2.2 Particle Size Distribution Analysis

A sieve analysis was performed to obtain the particle size distribution of Ottawa F65 sand. The analysis follows the ASTM D422 standard procedures. Five tests were performed on samples from different sand batches. Figure 3.2 shows the plot of the particle size distributions, while Table 3.2 shows a summary of test results.

Table 3.1 Specific gravity of Ottawa F65

Test	Batch #1	Batch #2	Batch #3	Batch #4	Batch #5
1	2.63	2.67	2.63	2.66	2.67
2	2.65	2.65	2.64	2.64	2.62
3	2.64	2.68	2.66	2.65	2.63
4	2.66	2.58	2.66	2.65	2.67
5	2.65	2.68	2.65	2.64	2.65
6	2.65	2.66	2.68	2.65	2.64
Mean	2.65	2.65	2.65	2.65	2.65
COV (%)	0.40	1.47	0.73	0.30	0.71

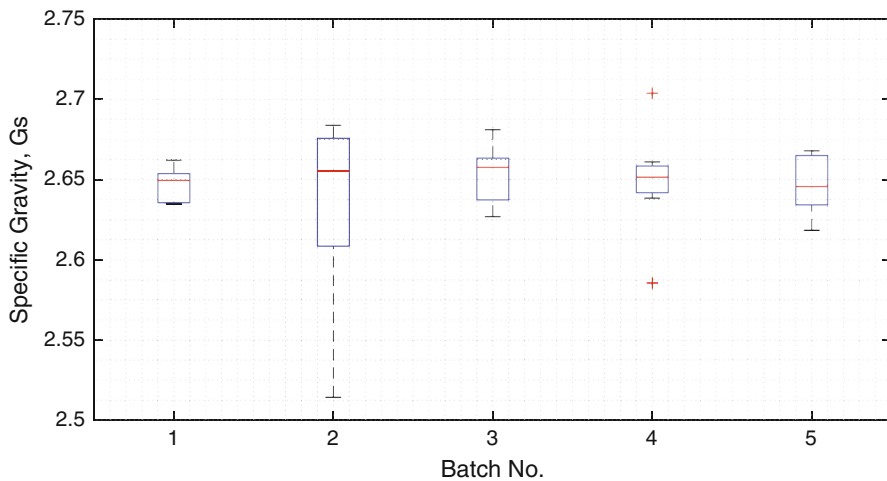
**Fig. 3.1** Ottawa F65 specific gravity test results

Figure 3.3 shows a comparison between the average distribution and the one obtained by Vasko in 2015. D_{10} , D_{30} , and D_{60} are indicated in Fig. 3.3, while the D_{50} values are presented in Table 3.3. The soil coefficient of uniformity, C_u , and coefficient of curvature, C_c , were 1.728 and 0.947, respectively. According to the Unified Soil Classification System, the soil is classified as poorly graded sand with designation SP.

3.2.3 Hydraulic Conductivity

A series of constant head hydraulic conductivity tests were conducted to determine the permeability of Ottawa F65 sand at different densities. The tests followed the ASTM D 2434 standard testing procedures. Table 3.4 shows the hydraulic conductivity for different initial void ratios. The hydraulic conductivity values presented are

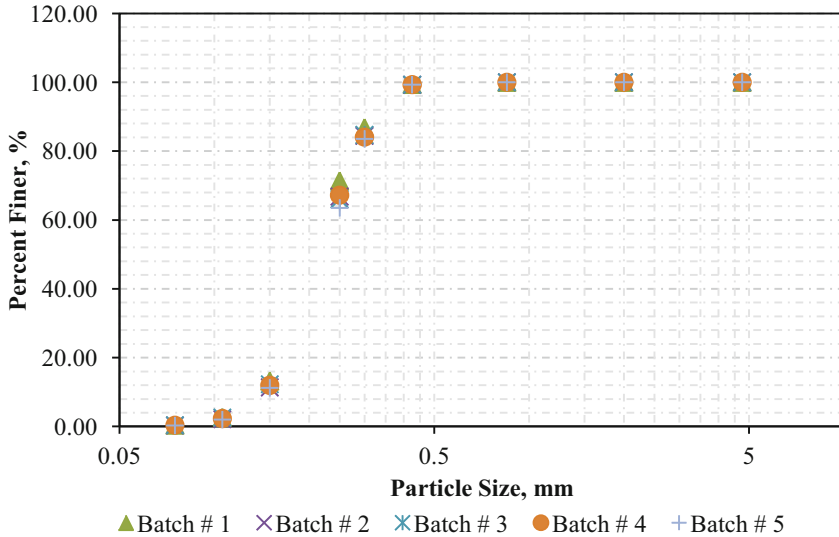


Fig. 3.2 Ottawa F65 particle size distribution

corrected to a temperature of 20 °C. The test samples were prepared using a constant height dry pluviation technique. The same technique was used for preparation of the soil samples for the triaxial experiments presented in the following section. Figure 3.4 shows a plot of the hydraulic conductivity versus the initial void ratio. The permeability reported here is in the same order of magnitude as the results reported by Vasko (2015) and Bastidas (2016). While the results obtained by Vasko (2015) fall within the range of values reported herein, the permeability reported by Bastidas (2016) was slightly higher.

3.2.4 Maximum and Minimum Void Ratios

Maximum and minimum void ratio tests were conducted on Ottawa F65 sand by different researchers. Table 3.5 shows the average values from the tests performed by the different groups (Kutter et al. 2017). Two different testing procedures were used in obtaining the maximum and minimum void ratios. The first is based on the ASTM standard testing procedures D4253 and D4254, while the second method is the one proposed by Lade et al. (1998). The results show a wide range of variation among the different reporting groups. The sources of variations are either inherent in the Ottawa F65 sand or caused by the testing procedures.

In order to improve our understanding of the causes of the variability observed in the maximum and minimum void ratio results, additional tests were conducted at GWU. The tests were performed using the method proposed by Lade et al. (1998). The tests were conducted by different researchers to address the human factor in the

Table 3.2 Particle size distribution of Ottawa F65

Sieve number	Diameter (mm)	Percent passing – P#1 (%)	Percent passing – P#2 (%)	Percent passing – P#3 (%)	Percent passing – P#4 (%)	Percent passing – P#5 (%)	Average percent passing (%)	Standard deviation (%)
4	4.75	100.00	100.00	100.00	100.00	100.00	100.	0
10	2	100.00	100.00	100.00	100.00	100.00	100.	0
20	0.85	100.00	100.00	100.00	100.00	100.00	100.	0
40	0.425	99.39	99.27	99.32	99.29	99.34	99.32	0.05
50	0.3	86.81	84.44	84.73	84.07	83.55	84.72	1.25
60	0.25	71.36	66.81	66.04	67.20	63.50	66.98	2.84
100	0.15	13.19	11.33	12.25	11.92	11.16	11.97	0.81
140	0.106	2.63	2.10	2.60	2.28	1.99	2.32	0.29
200	0.075	0.37	0.29	0.40	0.34	0.26	0.33	0.06

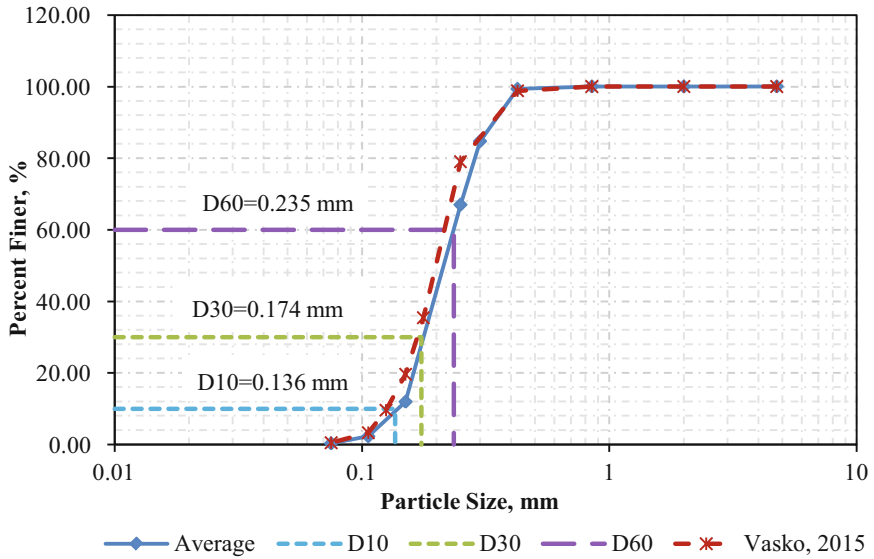


Fig. 3.3 Ottawa F65 average particle size distribution

Table 3.3 D50 of Ottawa F65 sand

	Sample 1	Sample 2	Sample 3	Sample 4	Sample 5	Vasko (2015)
D50, mm	0.21	0.21	0.21	0.21	0.22	0.2

Table 3.4 Hydraulic conductivity of Ottawa F65

Void ratio, e_o	Permeability, $T = 20\text{ }^\circ\text{C}$, cm/s	Void ratio, e_o	Permeability, $T = 20\text{ }^\circ\text{C}$, cm/s
0.571	0.010	0.702	0.012
0.697	0.011	0.706	0.014
0.668	0.012	0.713	0.016
0.590	0.010	0.697	0.012
0.476	0.009	0.644	0.010
0.766	0.015	0.650	0.015
0.699	0.012	0.653	0.014
0.486	0.008	0.646	0.014
0.674	0.013	0.642	0.016
0.721	0.015	0.622	0.014
0.694	0.014	0.494	0.011

results. Tables 3.6 and 3.7 show the mean, range, and coefficient of variation for a series of tests performed. The data sets 1 and 2 were obtained at GWU in 2017 by the authors, while data set 3 was the results of experiments by Vasko in 2015. Set 4 considers the range, mean, and coefficient of variation of the results presented in Table 3.5.

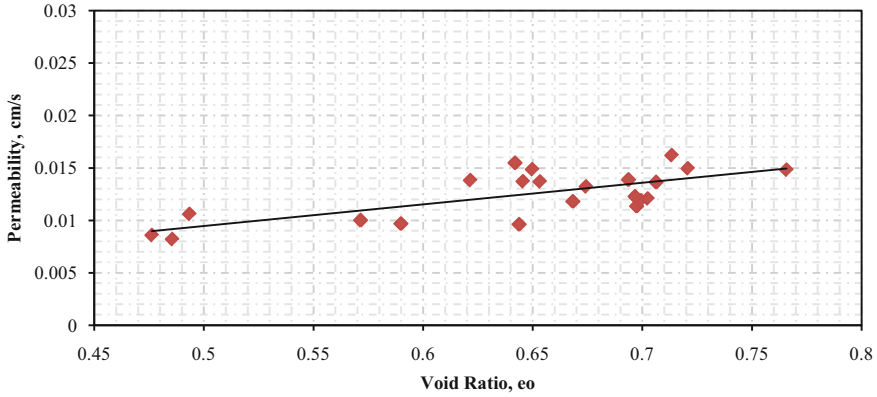


Fig. 3.4 Hydraulic conductivity, k , vs. void ratio, e_o

Table 3.5 Maximum and minimum void ratio obtained by different researchers (Kutter et al. 2017)

		$(\rho_{dry})_{min}$ kg/m ³	$(\rho_{dry})_{max}$ kg/m ³	e_{max}	e_{min}
Cooper Labs (UCD)	ASTM D4254 & ASTM D4253	1515	1736	0.75	0.53
GeoComp (RPI)	ASTM D4254 & ASTM D4253	1494	1758	0.77	0.51
Andrew Vasco (GWU)	ASTM D4253	1538	1793	0.72	0.48
Andrew Vasco (GWU)	Lade et al. (1998)	1521	1774	0.74	0.49
Eduardo Cerna (UCD)	Lade et al. (1998)	1415	1720	0.87	0.54
Wen-Yi Hung (NCU)	N/A	1482	1781	0.79	0.49
Yan-Guo Zhou (ZJU)	N/A	1456	1733	0.82	0.53

Table 3.6 Minimum void ratio

e_{min}	1	2	3	4
Max	0.519	0.521	0.522	0.581
Min	0.479	0.475	0.469	0.478
Average	0.500	0.501	0.491	0.515
COV (%)	2.7	2.8	3.7	6.8

Table 3.7 Maximum void ratio

e_{max}	1	2	3	4
Max	0.786	0.779	0.777	0.825
Min	0.712	0.729	0.702	0.723
Average	0.740	0.763	0.739	0.774
COV (%)	3.	2.	3.3	5.

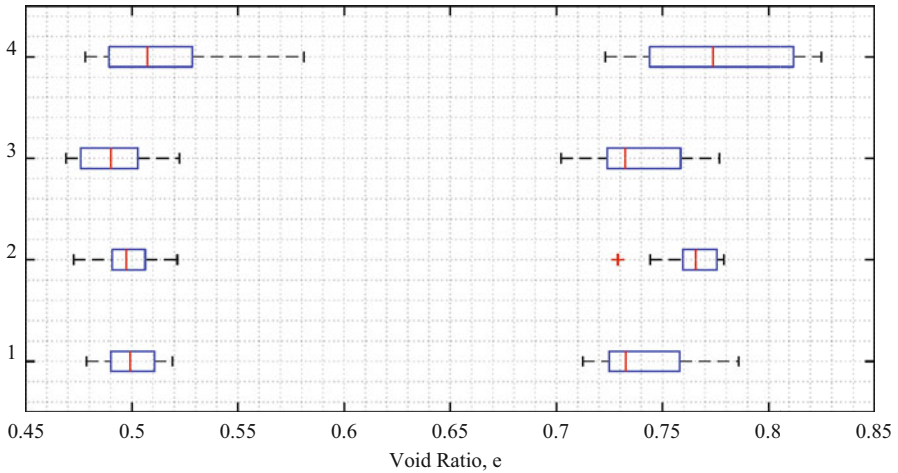


Fig. 3.5 Scatter of the maximum and minimum void ratios obtained by different experimenters

The scatter of the results is represented by a box plot in Fig. 3.5. It can be seen from the results that data sets 1–3 have a consistent range of variation while it is higher for data set 4. It can also be seen that there is a larger variation in the maximum void ratio than in the minimum void ratio.

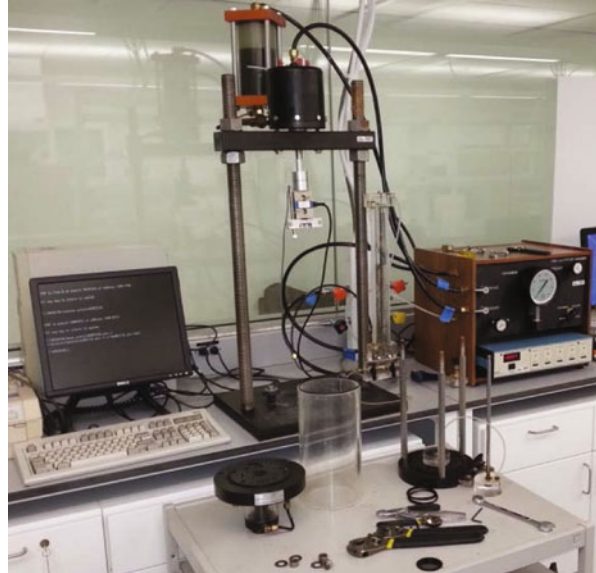
Carey et al. (2019) performed additional tests to obtain maximum and minimum void ratios on the samples obtained from the testing facilities that participated in LEAP 2017 project. These tests were also conducted using the same procedures as the ones employed in the tests reported in this paper. The results showed similar ranges of variation in the e_{\min} and e_{\max} . As a compromise, the median e_{\max} and e_{\min} values obtained by using the ASTM procedures were adopted for future analysis of LEAP data, where $e_{\max} = 0.78$ and $e_{\min} = 0.51$. These agreed upon values were adopted after the LEAP 2017 prediction exercise.

3.3 Cyclic Triaxial Tests

Stress-controlled tests were conducted on three different soil densities to evaluate the soil's liquefaction strength. The three soil densities have average initial void ratios of 0.585, 0.547, and 0.515. The experiment setup and procedures and the sample preparation technique are first discussed. Then, the results obtained are presented.

In this study the testing equipment used was the CKC e/p cyclic triaxial testing system manufactured by C.K. Chan at the Soil Engineering Equipment Company. The setup of the machine is shown in Fig. 3.6. The system is an electro-pneumatic system, which relies on in-house pressure for operation. Different testing conditions are permitted in this system including consolidation testing, monotonic stress/strain-controlled testing, and cyclic stress/strain-controlled testing among other tests.

Fig. 3.6 CKC e/p cyclic triaxial testing machine



3.3.1 Experiment Procedures

A cyclic triaxial experiment consists of sample preparation, saturation, consolidation, and shearing. In sample preparation the soil specimen is set up to match the target density. This step is the most critical to the consistency among experiments. Careful measurements have to be taken to reduce the variability in the results.

For the cyclic triaxial experiments performed in this study, the following steps were followed. First, the triaxial cell was cleaned and then dried using pressurized air. Then, a rubber membrane was placed around the bottom cap. The thickness of the membrane was measured from its top and bottom. Afterwards the triaxial mold was placed around the bottom cap and the membrane was stretched over the mold. Vacuum was then applied to the mold to hold the membrane onto it. At this point, the weight of the cell base, the mold, and the porous stones used was measured. Next, the sample was prepared using the *constant height dry pluviation* method to achieve a target density. Once, the sample was prepared, vacuum was applied to the soil specimen to hold its shape. The weight of the soil specimen, cell base, the mold, and porous stones was then measured. The difference between the two measurements of the weight yields the dry weight of the soil specimen. Then the dimensions of the soil specimen were taken including the diameter and the sample height at five different locations. From the measurement obtained, the volume of the specimen, the dry density, and the initial void ratio were computed.

Figure 3.7 shows the prepared soil specimen subjected to vacuum and attached to the triaxial base and top cap. The statistics obtained on the measurements of the sample dimensions and weight are shown in Table 3.8. It can be seen from the results

Fig. 3.7 Prepared sample subject to vacuum



Table 3.8 Statistics of soil specimens

Measurement	Mean	COV (%)
Height, mm	164.64	0.24
Diameter, mm	71.14	0.18
Weight ($e_o = 0.515$), g	1142.3	0.30
Weight ($e_o = 0.547$), g	1120.3	0.42
Weight ($e_o = 0.585$), g	1089.0	0.51

in the table that the coefficient of variations for the specimen measurements was below 1%. Figures 3.8, 3.9, and 3.10 show the cumulative distribution for the sample weight, height, and diameter. The distribution of the measured data can be fitted using a normal distribution as can be seen in the figures. While Fig. 3.8 shows the distribution of the sample weight for each void ratio separately, Figs. 3.9 and 3.10 combines the measurements of all the tests specimen for the sample height and diameter.

Once the sample was prepared, then it was enclosed with the cell chamber. The sample was then saturated with de-aerated water. Figure 3.11 shows the saturation

Fig. 3.8 Experimental and fitted cumulative distribution of the sample weight data

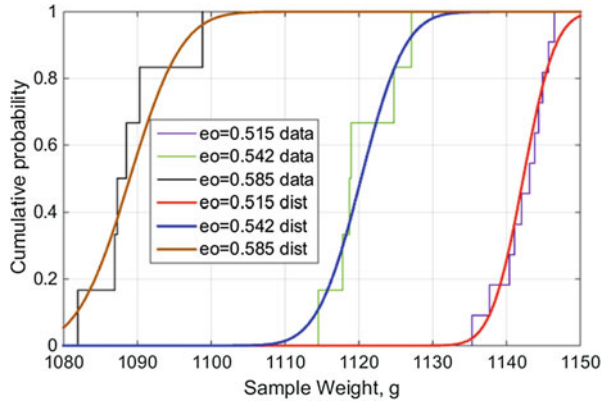


Fig. 3.9 Experimental and fitted cumulative distribution of the sample height data

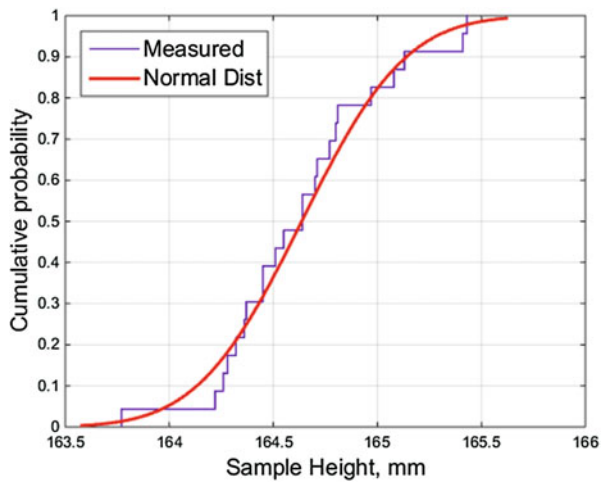


Fig. 3.10 Experimental and fitted cumulative distribution of the sample diameter data

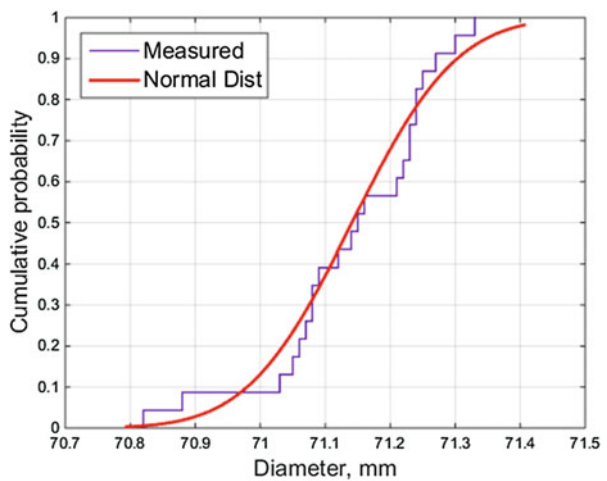
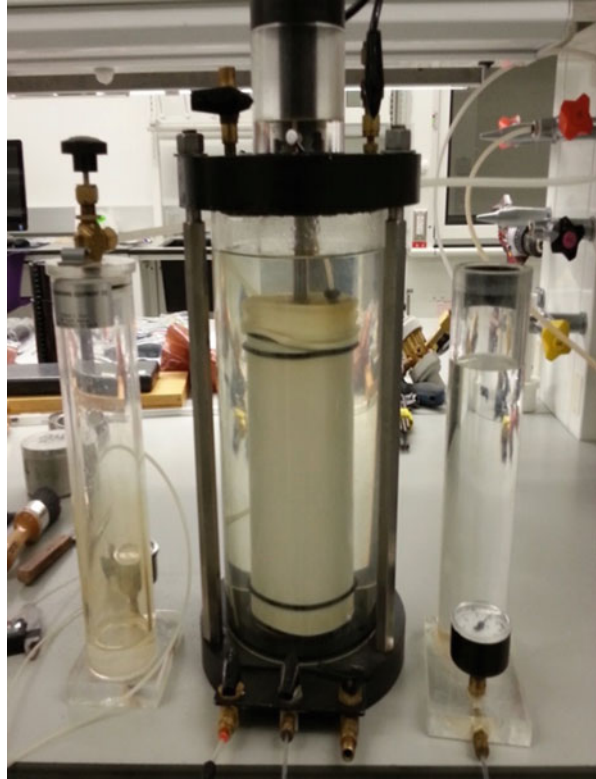


Fig. 3.11 Saturation of test specimen



setup which was composed of two containers. The first container was filled with the de-aerated water and connected to the bottom of the soil specimen. The second one was subjected to vacuum and connected to the top of the specimen. The saturation step continued until there were no air bubbles coming in to the vacuumed container. After this step was completed, the triaxial cell was attached to the load frame and the pressure tubes were connected to the soil specimen and the chamber.

Once the specimen was connected to the machine, the testing sequence began. First the specimen was subjected to back pressure saturation. Pressure increments of 10 kPa were gradually applied until a B value greater than 0.95 was achieved. Next, the specimen was consolidated to an effective confining pressure of 100 kPa for 45 min. At the end of the consolidation, the volumetric strain developed was obtained and the void ratio was updated. Subsequently, the specimen was subjected to the cyclic shear stress that matches the target cyclic stress ratio (CSR). In the shearing step, the load was applied at a period of 1 min/cycle for the denser specimens with void ratios of 0.515 and 0.542, while a frequency of 3 min/cycle was used for the looser specimens with a void ratio of 0.585.

3.3.2 Sample Preparation

A constant height dry pluviation method was used for the sample preparation. In such method the target density of the sample is achieved by pouring the sand into the mold from a specific height. In order to create a more uniform sample, a constant height of drop should be maintained between the sample surface and hopper. In order to produce samples with similar fabric and consistency, two types of sand pluviators were considered.

The first pluviator, Fig. 3.12, was used for preparing the sample with void ratio of 0.515 ($\rho_d = 1774.2 \text{ kg/m}^3$). The pluviator is composed of a sand hopper with a top diameter of 24 cm and total depth of 21 cm. The exit diameter of the hopper is 7.5 cm. The exit of the bucket is covered with a shutter plate with 13 openings. Each opening has a diameter of 0.5 cm. The end of the pluviator has a number 8 sieve with a mesh opening of 2.36 mm. The distance between the sieve and the shutter plate is 15.0 cm. The drop height of the sand (distance from the sieve to the surface of the deposited sand) is 19.8 cm. In order to control the flow rate of the sand and the uniformity of the sand placed in the pluviator, a dispersion cup hanging from the top of the pluviator is used to place the sand in the hopper with a consistent and uniform density.

The second pluviator, Fig. 3.13, was used for preparation of specimen with initial void ratios 0.585 ($\rho_d = 1665.6 \text{ kg/m}^3$) and 0.542 ($\rho_d = 1712.6 \text{ kg/m}^3$). The pluviator is composed of a hopper with the same dimensions as pluviator 1 with a diameter of 24.0 cm and depth of 21 cm. The distance from the exit of the hopper to the end of

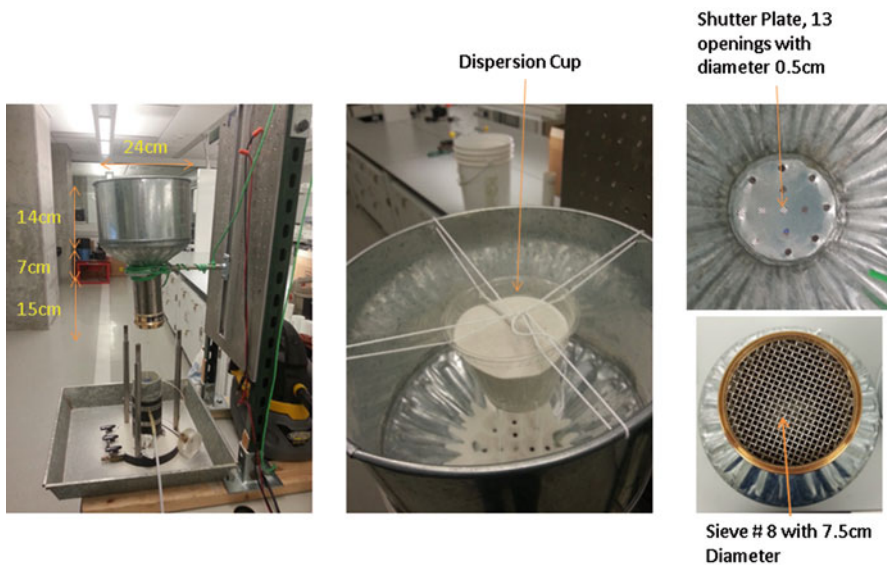


Fig. 3.12 Sample pluviator 1

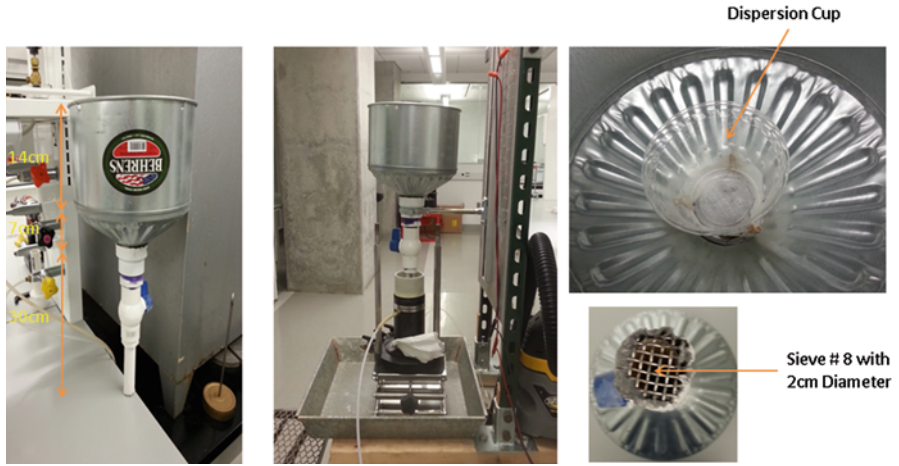


Fig. 3.13 Sample pluviator 2

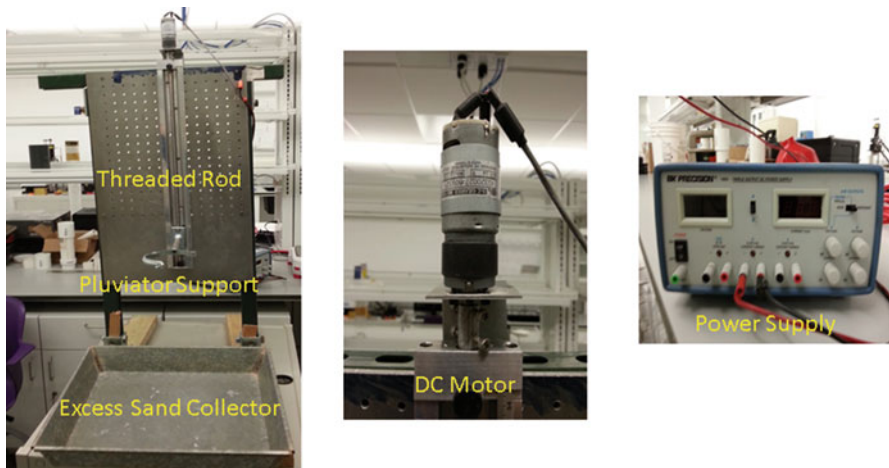


Fig. 3.14 Pluviator lift

the pluviator is 30 cm. The end of the pluviator has an opening of 2.0 cm, and it is covered with a number 8 sieve. The drop height is 2.0 cm and 4.0 cm for samples with void ratio of 0.585 and 0.542, respectively. A dispersion cup is used for sample uniformity and flow rate control.

In order to maintain a constant height during the sample preparation, a pluviator lift, Fig. 3.14, was used. The pluviator lift is composed of a support for the sample pluviator. The support is attached to a steel frame, and it is moved upwards and downwards through a threaded rod. The movement of the threaded rod is controlled

by a DC motor. The speed of the motor is controlled by a power supply. During the sample preparation, the sand is gradually deposited until it flows from the surface of the mold. Afterwards the sample surface is leveled in order to ensure a consistent sample height. The excess sand is collected in the sand collector.

3.3.3 Summary of Experimental Results and Observations

Three sets of experiments were conducted with the following void ratios of 0.515, 0.542, and 0.585 ($\rho_d = 1744.2, 1712.6, 1665.6 \text{ kg/m}^3$). As it was shown in the previous section (Tables 3.5 and 3.6), the reported maximum and minimum void ratios for Ottawa F65 sand by various methods have significant variability that causes a significant uncertainty in the computed relative density for a given void ratio. Table 3.9 summarizes the computed relative density for each achieved void ratio based on the average reported maximum and minimum void ratios. It can be seen from the results in Table 3.9 that the relative density corresponding to the achieved void ratio can have a coefficient of variation of about 12%.

In Fig. 3.15 the results obtained from one of the cyclic triaxial tests are presented. The sample tested is a dense sample with an initial void ratio of 0.515 and a confining stress of 100 kPa. The specimen is subjected to a cyclic shear stress with a cyclic stress ratio ($\text{CSR} = \sigma_d/2\sigma'_3$) of 0.325. The effective stress path, the stress

Table 3.9 Relative density of tested specimen according to the reported e_{\min} and e_{\max}

Tested by	Institute	ρ_{\min} kg/m ³	ρ_{\max} kg/m ³	e_{\max}	e_{\min}	$e = 0.515$	$e = 0.542$	$e = 0.585$
						Dr (%)	Dr (%)	Dr (%)
Mohamed El Ghoraiby	GWU	1503	1765	0.76	0.5	94.8	84.5	68.1
Hannah Park	GWU	1523	1767	0.74	0.5	93.6	82.4	64.5
Andrew Vasko	GWU	1524	1777	0.74	0.49	90.4	79.5	62.1
Andrew Vasko	GWU	1538	1793	0.72	0.48	84.9	73.9	56.3
Eduardo Cerna	UC Davis	1415	1720	0.87	0.54	107.7	99.6	86.7
Cooper Labs	UC Davis	1515	1736	0.75	0.53	105.2	93.0	73.7
Wen-Yi Hung	NCU	1482	1781	0.79	0.49	91.0	82.0	67.7
GeoComp	RPI	1494	1758	0.77	0.51	97.1	87.0	70.9
Yan-Guo (Eagle) ZHOU	ZJU	1456	1733	0.82	0.53	104.9	95.6	80.8
Ana Maria Parra Bastidas	UC Davis	1455	1759	0.82	0.51	97.3	88.7	75.1
Carey et al. (2019)	Various	1491	1757	0.78	0.51	97.5	87.5	71.5
Average						96.8	86.7	70.7
COV						7.2	8.6	12

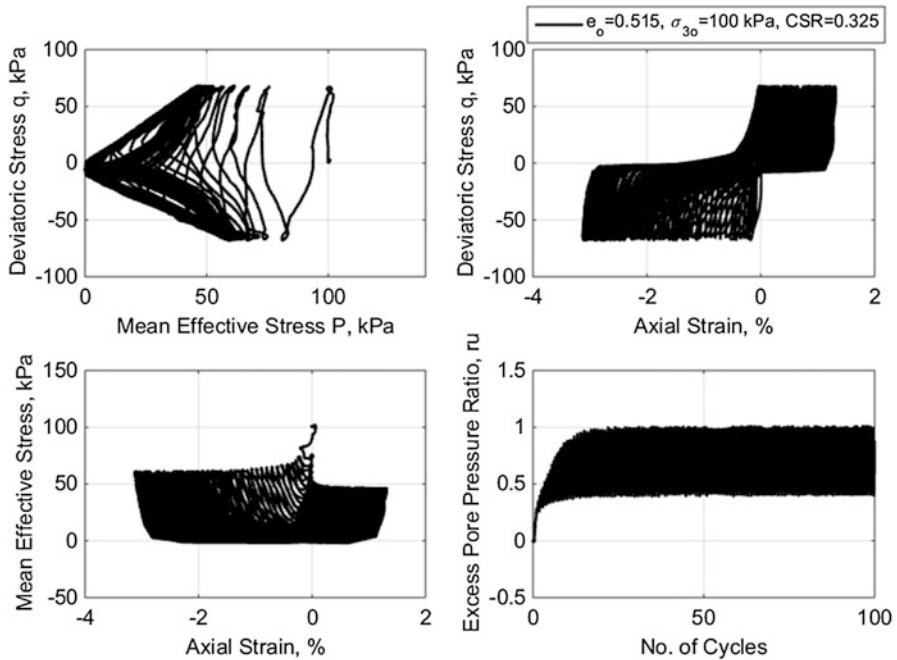


Fig. 3.15 Triaxial experiment results of Ottawa F65 sand specimen with void ratio of 0.515 and CSR of 0.325

Table 3.10 Summary of experiments on specimen with $e_o = 0.515$

$e_o = 0.515 - \rho_d = 1744.2 \text{ kg/m}^3$							
Date	e_a	e_o	B	e_s	CSR	2.5% s.a.	$r_u = 1.0$
10/10/2016	0.522	0.515	0.971	0.499	0.600	14	15.53
10/6/2016	0.526	0.522	0.953	0.506	0.500	17	26
10/7/2016	0.517	0.512	0.977	0.497	0.450	19	15.55
9/16/2016	0.520	0.515	0.962	0.500	0.375	26	25
9/27/2016	0.518	0.514	0.952	0.501	0.365	29	16
9/30/2016	0.512	0.507	0.959	0.494	0.325	41	18
9/22/2016	0.518	0.514	0.950	0.502	0.315	46	37
9/28/2016	0.521	0.516	0.951	0.500	0.300	48	31
9/13/2016	0.522	0.517	0.961	0.505	0.275	60	35
9/29/2016	0.520	0.515	0.959	0.503	0.265	70	45
10/12/2016	0.517	0.513	0.951	0.501	0.225	191	140

strain response, the mean effective stress vs. strain response, and the excess pore pressure development are shown. It can be seen that the response of the soil specimen follows a typical cyclic mobility pattern. The liquefaction strength of the soil is measured based on the number of cycles to achieve a certain level of shear strain. In this study, the criterion is taken to be the number of cycles to develop a single amplitude shear strain of 2.5%. Tables 3.10, 3.11, and 3.12 show a summary

Table 3.11 Summary of experiments on specimen with $e_o = 0.542$

$e_o = 0.542 - \rho_d = 1712.6 \text{ kg/m}^3$							
Date	e_a	e_o	B	e_s	2.5% s.a.	$r_u = 1.0$	CSR
11/20/2016	0.556	0.550	0.956	0.539	16	12	0.28
11/18/2016	0.545	0.540	0.96	0.529	18	16	0.24
11/16/2016	0.540	0.535	0.958	0.523	22	14	0.22
11/16/2016	0.544	0.538	0.973	0.527	28	25	0.21
11/16/2016	0.555	0.550	0.971	0.533	41	36	0.2
11/21/2016	0.544	0.538	0.958	0.524	50	41	0.19

Table 3.12 Summary of experiments on specimen with $e_o = 0.585$

$e_o = 0.585 - \rho_d = 1665.6 \text{ kg/m}^3$							
Date	e_a	e_o	B	e_s	CSR	2.5% s.a.	$r_u = 1.0$
11/10/2016	0.589	0.581	0.955	0.57	0.2	9	9
11/1/2016	0.592	0.584	0.963	0.562	0.17	15	13
11/2/2016	0.592	0.587	0.953	0.567	0.16	17	16
11/4/2016	0.581	0.575	0.955	0.557	0.14	33	31
11/7/2016	0.605	0.598	0.958	0.581	0.12	59	58
11/14/2016	0.588	0.583	0.954	0.566	0.10	188	186

Table 3.13 Statistics of experiments on specimen with $e_o = 0.515$

	e_a	e_o	B	e_s
Mean	0.519	0.515	0.959	0.501
SD	0.004	0.004	0.009	0.003
COV (%)	0.696	0.703	0.918	0.681

Table 3.14 Statistics of experiments on specimen with $e_o = 0.542$

	e_a	e_o	B	e_s
Mean	0.547	0.542	0.963	0.529
SD	0.007	0.007	0.007	0.006
COV (%)	1.199	1.204	0.765	1.136

of the experiments performed for each initial void ratio. The tables show the achieved sample void ratio after pluviation (e_a), consolidation (e_o), and shearing (e_s) the test specimens. The number of cycles until 2.5% single amplitude (s.a.) of strain and until an excess pore pressure ratio of 1.0 are first achieved is shown. Tables 3.13, 3.14, and 3.15 show the statistics of the void ratios and the B values achieved. Figure 3.16 shows the liquefaction strength curves obtained for the three soil densities tested. The results of each experiment are archived in a databank on DesignSafe allowing for public access (El Ghoraiby et al. 2018).

While the curves shown in Fig. 3.16 have been used to describe the liquefaction strength of the soil, they only represent a single snapshot of the soil response at the

Table 3.15 Statistics of experiments on specimen with $e_o = 0.585$

	e_a	e_o	B	e_s
Mean	0.591	0.585	0.956	0.567
SD	0.008	0.008	0.004	0.008
COV (%)	1.334	1.310	0.384	1.434

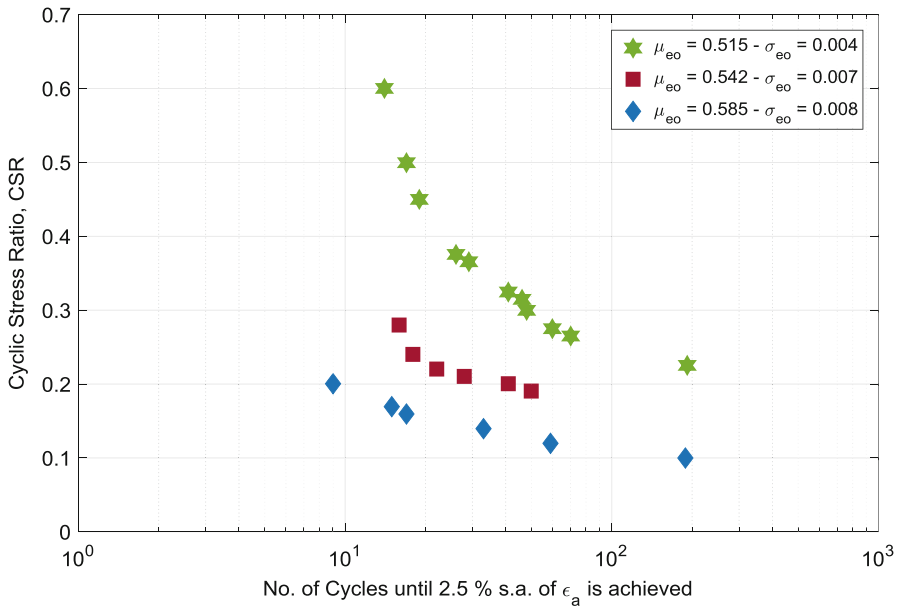


Fig. 3.16 Liquefaction strength curves for Ottawa F65 sand

end of the tests. In order to gain more insight on the progression of the soil response, additional information were obtained by counting the number of cycles it took to reach different levels of shear strain. Figures 3.17, 3.18, and 3.19 show the strength curves corresponding to a range of strains (0.5–2.5%) for the soil specimens with initial void ratios of 0.585, 0.542, and 0.515, respectively. It can be seen that as the soil density increases, the number of shear cycles required to move from one shear strain level to the next level increases.

It is also useful to observe the progression of the soil response in terms of excess pore water pressure ratio, r_u . Figures 3.20, 3.21, and 3.22 show the variation of number of shear stress cycles required to reach certain levels of r_u (in the range of 0.7–0.99) for the samples with initial void ratios of 0.585, 0.542, and 0.515, respectively. It is observed that as the soil density increases the number of shear stress cycles required to generate certain levels of excess pore pressure ratio increases. For the loosest sand, the number of cycles to reach $r_u = 0.7$ is slightly less than the number of cycles to reach $r_u = 0.99$. For the denser sand, the number of cycles to reach $r_u = 0.7$ is much less than the number of cycles to reach $r_u = 0.99$.

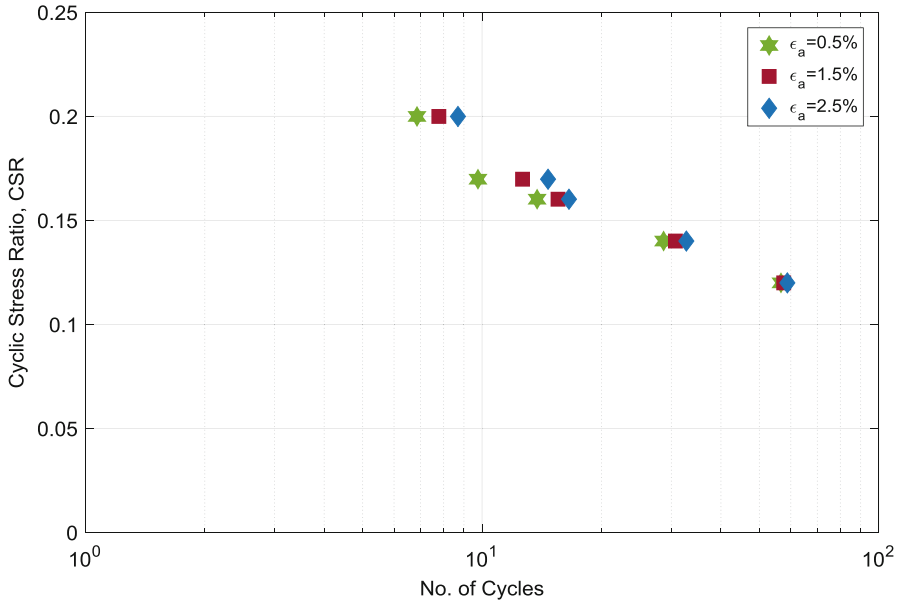


Fig. 3.17 Strength curves for different axial strain amplitudes— $e_o = 0.585$

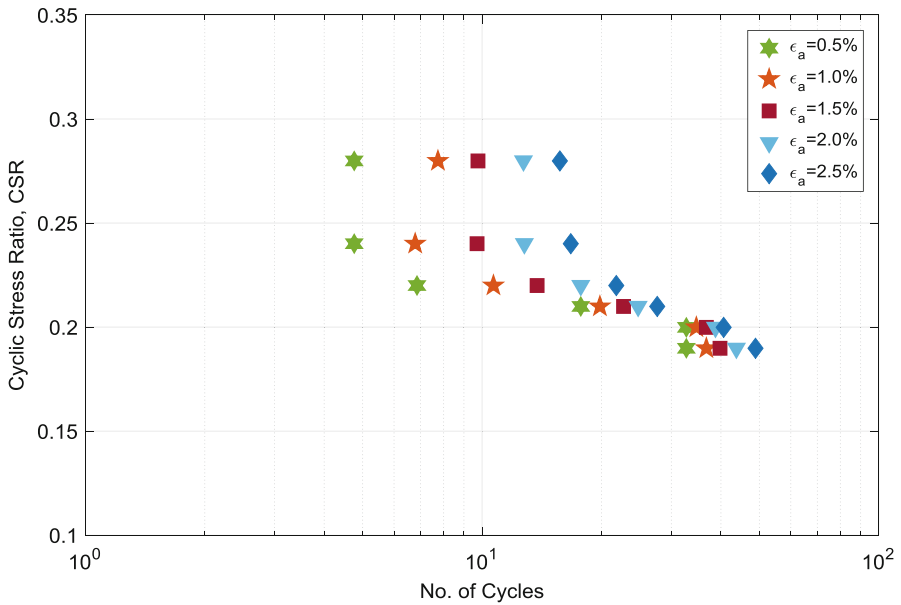


Fig. 3.18 Strength curves for different axial strain amplitudes— $e_o = 0.542$

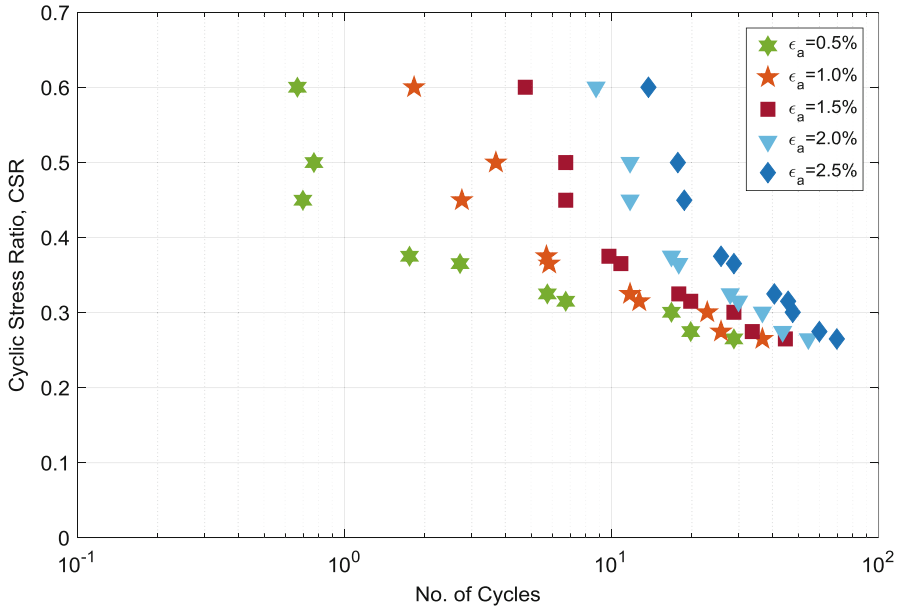


Fig. 3.19 Strength curves for different axial strain amplitudes— $e_o = 0.515$

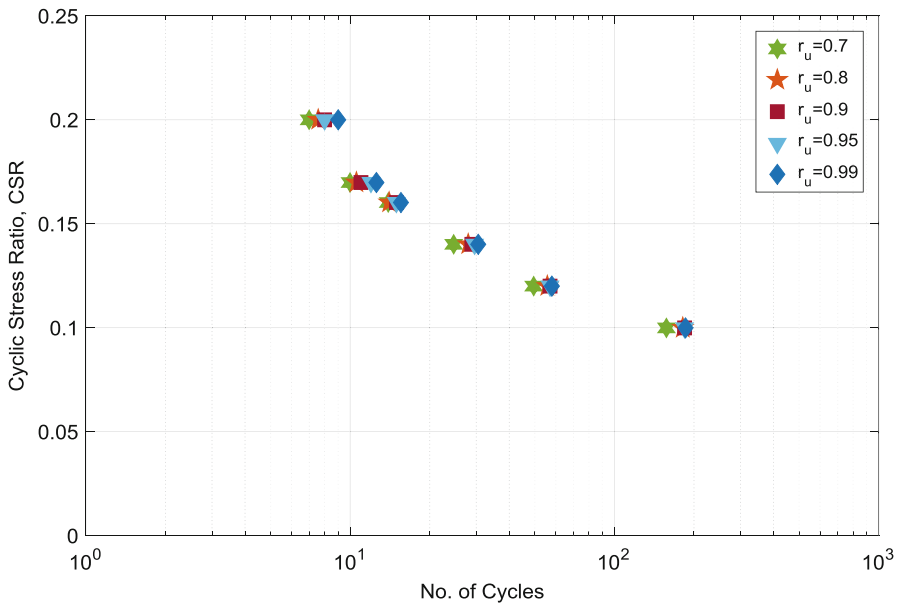


Fig. 3.20 Strength curves for different excess pore pressure ratios— $e_o = 0.585$

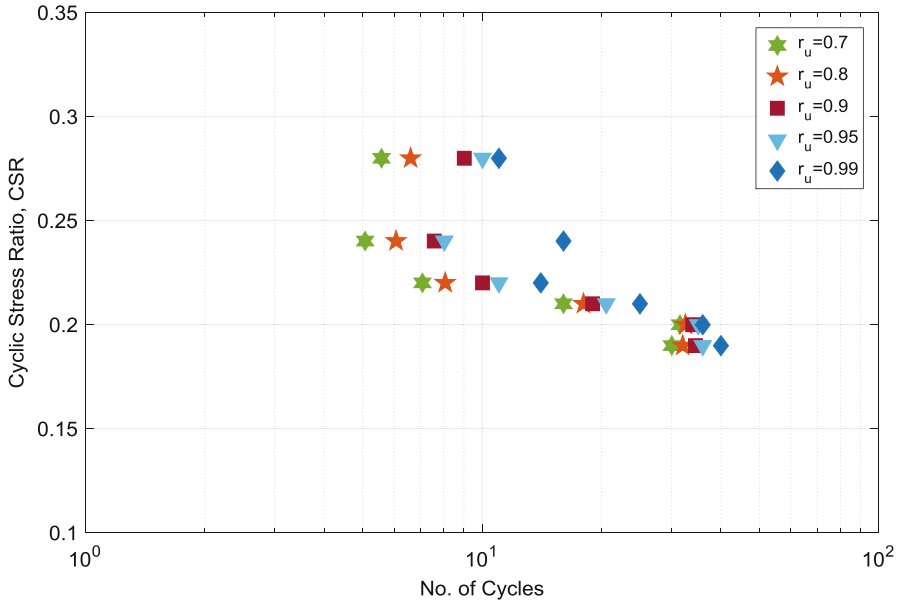


Fig. 3.21 Strength curves for different excess pore pressure ratios— $e_o = 0.542$

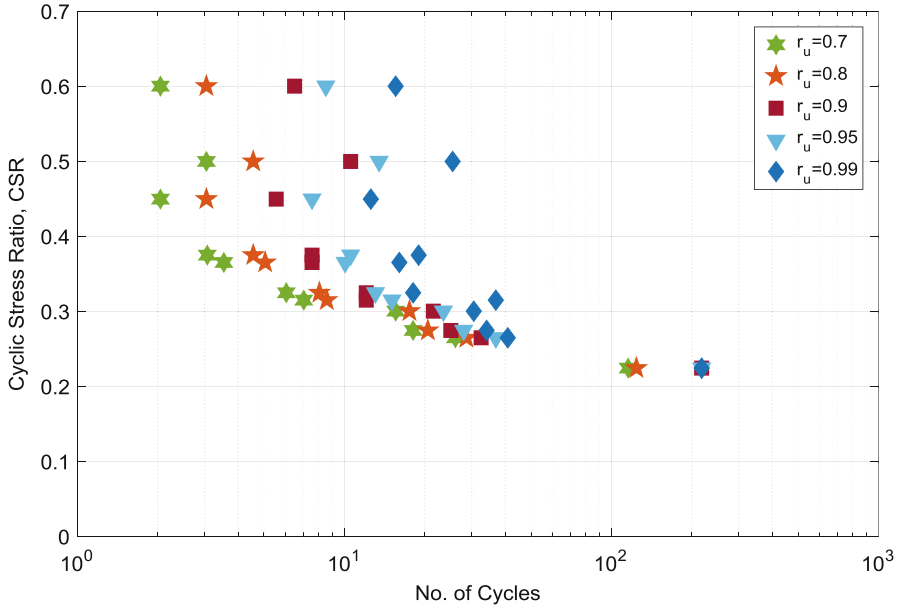


Fig. 3.22 Strength curves for different excess pore pressure ratios— $e_o = 0.515$

3.4 Concluding Remarks

A series of laboratory experiments were conducted to characterize the physical and mechanical properties of Ottawa F65 sand. A large number of experiments were performed to obtain specific gravity, particle size distribution, maximum and minimum void ratios, hydraulic conductivity, and stress-strain-strength behavior of Ottawa sand. The results of 23 cyclic triaxial tests were reported for three different initial void ratios. The results of cyclic triaxial tests are presented in form of liquefaction strength curves. A databank of this experimental study has been created and uploaded on DesignSafe (El Ghoraiby et al. 2018).

References

- Bastidas, A. M. B. (2016). *Ottawa F-65 sand characterization*. Davis, CA: University of California.
- Carey, T. J., Stone, N., & Kutter, B. L. (2019). Grain size analysis and maximum and minimum dry density of Ottawa F-65 sand for LEAP-UCD-2017. In B. Kutter et al. (Eds.), *Model tests and numerical simulations of liquefaction and lateral spreading: LEAP-UCD-2017*. New York: Springer.
- El Ghoraiby, M. A., Park, H., & Manzari, M. (2018). *LEAP-2017 GWU Laboratory Tests*. DesignSafe-CI, Dataset. <https://doi.org/10.17603/DS2210X>.
- Kutter, B. L., Carey, T. J., Hashimoto, T., Zeghal, M., Abdoun, T., Kokkali, P., Madabhushi, G., Haigh, S. K., Burali d'Arezzo, F., Madabhushi, S., Hung, W.-Y., Lee, C.-J., Cheng, H.-C., Iai, S., Tobita, T., Ashino, T., Ren, J., Zhou, Y.-G., Chen, Y.-M., Sun, Z.-B., & Manzari, M. T. (2017). LEAP-GWU-2015 experiment specifications, results, and comparisons. *Soil Dynamics and Earthquake Engineering*, 4, 1–31.
- Lade, P. V., Liggio, C. D., & Yamamuro, J. A. (1998). Effects of non-plastic fines on minimum and maximum void ratios of sand. *Geotechnical Testing Journal*, 21(4), 336–347.
- Manzari, M. T., ElGhoraiby, M., Kutter, B. L., Zeghal, M., Abdoun, T., Arduino, P., Armstrong, R. J., Beaty, M., Carey, T., Chen, Y., Ghofrani, A., Gutierrez, D., Goswami, N., Haigh, S. K., Hung, W.-Y., Iai, S., Kokkali, P., Lee, C.-J., Madabhushi, S. P. G., Mejia, L., Sharp, M., Tobita, T., Ueda, K., Zhou, Y., & Ziotopoulou, K. (2017). Liquefaction experiment and analysis projects (LEAP): Summary of observations from the planning phase. *Soil Dynamics and Earthquake Engineering*. <https://doi.org/10.1016/j.soildyn.2017.05.015>
- Vasko, A. (2015). *An investigation into the behavior of Ottawa sand through monotonic and cyclic shear tests*. Washington: George Washington University.
- Vasko, A., ElGhoraiby, M. A., & Manzari, M. T. (2018). *LEAP-GWU-2015 Laboratory tests*. DesignSafe-CI, Dataset. <https://doi.org/10.17603/DS2TH7Q>.

Open Access This chapter is licensed under the terms of the Creative Commons Attribution 4.0 International License (<http://creativecommons.org/licenses/by/4.0/>), which permits use, sharing, adaptation, distribution and reproduction in any medium or format, as long as you give appropriate credit to the original author(s) and the source, provide a link to the Creative Commons license and indicate if changes were made.

The images or other third party material in this chapter are included in the chapter's Creative Commons license, unless indicated otherwise in a credit line to the material. If material is not included in the chapter's Creative Commons license and your intended use is not permitted by statutory regulation or exceeds the permitted use, you will need to obtain permission directly from the copyright holder.

